Gradient Descent-Based Online Mutual Inductances Identification and Transfer Route Optimization for Dynamically Reconfigurable WPT Network

Xiaomin Wang, Xin Dai, *Member, IEEE*, Shunsheng Hong, Yanling Li, and Udaya Kumara Madawala, *Fellow, IEEE*

***Abstract*—Wireless Power Transfer Network (WPTN), with their multidimensional dynamic magnetic coupling capabilities, address the limitations of traditional wireless power transfer (WPT) technologies in terms of degrees of freedom, thus advancing the development and application of WPT technologies. Accurate mutual inductance identification is essential for establishing and optimizing paths in WPTN systems. However, the dynamic nature of the network causes frequent changes in mutual inductance parameters as nodes join or leave. This makes traditional calculation methods inadequate for complex multinode network. To address this challenge, this article proposes a dynamic mutual inductance identification method based on the gradient descent algorithm. The method effectively handles simultaneous changes in multiple mutual inductance parameters caused by network topology variations. By constructing a mathematical model of the WPTN system and designing a gradient descent algorithm with adaptive learning rates, the method achieves synchronous identification of multiple mutual inductance parameters. It does not require pretraining or extensive computational resources, and supports both online and offline identification. Experimental results on a four-node system platform show that the proposed method can identify three new mutual inductances in real time during node switching, while dynamically selecting the most efficient transmission path.**

***Index Terms*—Dynamically reconfigurable wireless power transfer network (WPTN), gradient descent algorithm, mutual inductances identification, route optimization.**

I. Introduction

WIRELESS power transfer (WPT), as an emerging power supply technology, has been widely applied in various fields such as smart homes, medical electronics, drones, electric vehicles, and underwater equipment [1], [2], [3], [4], [5]. With the advancement of this technology, traditional one-to-one WPT systems can no longer meet the current demands for transmission distance and charging multiple electrical devices. To overcome these limitations, researchers have explored multinode WPT systems [6], [7], [8], including one-to-many or many-to-one systems. In recent years, more complex Wireless Power Transfer Network (WPTN) have become a research focus. Unlike multinode WPT systems, WPTN not only have multiple transmitting and receiving coils simultaneously, but also introduce relay coils to construct diverse power transfer paths, enhancing the spatial freedom of power transfer [9], [10]. However, this networked structure also brings more challenges, including the dynamic mutual inductance identification between nodes.

Existing research on WPTN systems primarily focuses on extending the power transfer distance [11], improving system output power and efficiency [12], and optimizing power transfer paths [13]. Most of these studies assume clear knowledge of mutual inductances between nodes. However, in practical applications such as Automated Guided Vehicle (AGV) cluster charging in factories, dynamic node insertion or removal and node function switching inevitably lead to changes in mutual inductances between nodes. Particularly in network with numerous nodes, changes in one node can simultaneously affect multiple mutual inductance parameters, subsequently impacting the stability and efficiency of the power transfer paths. Therefore, accurate mutual inductance identification is necessary to maintain reliability and efficiency when node changes occur.

Currently, mutual inductance identification methods primarily focus on traditional one-to-one WPT systems and can be broadly categorized into two approaches: 1) Mathematical modeling with signal analysis. This approach calculates mutual inductances by steady-state or transient analysis of input–output voltages and currents to establish mathematical models. For instance, Dai et al. [14] estimated coupling coefficients by analyzing variations in input–output signals and duty cycles. Wang et al. [15] calculated mutual inductances by inverting voltage and current values during system soft-start when the rectifier bridge is off; Hu et al. [16] employed Fourier transform methods to obtain the fifth harmonic amplitudes for calculating mutual inductances. Zeng et al. [17] performed frequency sweeps at the

Received 29 April 2025; revised 30 July 2025; accepted 23 September 2025. Date of publication 29 September 2025; date of current version 13 November 2025. This work was supported in part by the National Natural Science Foundation of China under Grant 52277003 and in part by the Fundamental Research Funds for the Central Universities under Grant 2022CDJQY-006 and Grant 2024CDJXY027. Recommended for publication by Associate Editor A. Barrado. *(Corresponding author: Xin Dai.)*

Xiaomin Wang, Xin Dai, and Shunsheng Hong are with the College of Automation, Chongqing University, Chongqing 400044, China (e-mail: 20221301001@stu.cqu.edu.cn; daixin@cqu.edu.cn; 20231301015@stu.cqu.edu.cn).

Yanling Li is with the School of Electrical Engineering and Electronic Information, Xihua University, Chengdu 610039, China (e-mail: yanling.li@mail.xhu.edu.cn).

Udaya Kumara Madawala is with the Department of Electrical Computer and Software Engineering, University of Auckland, Auckland 1010, New Zealand (e-mail: u.madawala@auckland.ac.nz).

Color versions of one or more figures in this article are available at https://doi.org/10.1109/TPEL.2025.3615389.

Digital Object Identifier 10.1109/TPEL.2025.3615389

transmitter side to detect system resonant frequencies, indirectly determining mutual inductances. However, this method only operates offline and is unsuitable for dynamically changing systems. Yue et al. [18] and Su et al. [19] achieved online mutual inductance identification based on time-domain mathematical modeling and steady-state harmonic analysis, respectively. Liu et al. [20] derived a nonlinear function set involving nine unknown parameters, including mutual inductance, output voltage, compensation capacitance, and fundamental and third harmonic coefficients of receiver coil current. Newton's iterative method calculates the mutual inductance, but this involves substantial computational effort. Wang et al. [21] improved real-time identification by employing adaptive filtering algorithms. 2) Circuit structure modification and hardware enhancement. This method directly or indirectly measures mutual inductances through additional auxiliary circuits, sensors, or system topology modifications. For example, Liu and Feng [22] added a T-shaped impedance matching network at the receiving end to calculate mutual inductances based on equivalent impedance. Sheng and Shi [23] introduced an auxiliary inverter at the transmitter to generate beat-frequency signals for envelope analysis and mutual inductance identification. Yang et al. [24] integrated a current sensor at the transmitter to measure mutual inductance based on the phase difference between transmitter current and reflected signals, although this approach requires temporarily short-circuiting the receiver.

Although the methods mentioned above have achieved success in conventional one-to-one systems, their effectiveness in multinode network environments is limited due to complexities related to node quantity and network topology. Existing studies addressing mutual inductance identification in multicoil WPT systems are scarce and mostly focused on three-coil systems. Yue et al. [25] established a frequency-domain model for an LCC-C compensated WPT system consisting of two transmitting coils and one receiving coil, using the Levenberg–Marquardt algorithm to iteratively calculate mutual inductances. Liu et al. [26] adjusted the relay coil compensation capacitance to change the system input impedance and calculate mutual inductances, but accuracy is directly influenced by tolerance limitations in relay coil compensation capacitors when operating under nonresonant conditions. Yang et al. [27] employed a two-layer Adaptive Differential Evolution (ADE) algorithm to identify mutual inductances and load for SS-type two-coil and three-coil WPT systems. Kim et al. [28] calculated mutual inductances among multiple transmitters and a single receiver by detecting reflected impedances, coil currents, and dc input voltages and currents. Based on Kim et al. [28] and Kim and Ahn [29] dynamically adjusts transmitter current ratios via mutual inductance proportion control to achieve maximum efficiency point tracking, although this method is limited to single-receiver scenarios. Zhu et al. [30] identified mutual inductances by sequentially switching nodes in multi-to-multi systems, but the method only supports offline identification and is unsuitable for systems incorporating relay coils.

In summary, existing research lacks effective methods for identifying multiple mutual inductances in WPTN under dynamic node variation scenarios. Specifically, current methods become complicated and computationally demanding when applied to high-order, nonlinear WPTN systems with numerous nodes, making it difficult to efficiently address the mutual inductance identification problem resulting from dynamic node insertion or removal. To overcome these challenges, this article proposes a dynamic multinode mutual inductance identification method based on gradient descent. This method breaks through the limitations of traditional analytical approaches, avoiding the complexity associated with solving high-order nonlinear equations. Specifically, the proposed method offers the following advantages.

1) A gradient descent-based online identification method for multiple coupled mutual inductances is proposed for WPTN with complex coupling relationships. The method can track dynamic topology changes in real time as nodes join or leave the network. It overcomes the limitations of traditional impedance matching methods, which cannot synchronously identify multiple mutual inductance parameters in complex network topologies.
2) Based on the real-time identified mutual inductance parameters, an efficiency-oriented transmission path optimization method is developed. This method enables dynamic adjustment of the network topology and reconstruction of transmission paths, maximizing system power transfer efficiency while ensuring power supply stability.

The rest of this article is organized as follows. Section II analyzes the mathematical model of the WPTN system. Section III proposes a method for synchronous identification of multiple mutual inductances based on the gradient descent algorithm and introduces the control strategy for the path optimization process. Section IV validates the feasibility and accuracy of the multimutual inductance identification method in WPTN through experiments. Finally, Section V concludes this article.

II. WPTN System Modeling

A. Node Functional Roles and Network Architecture in WPTN

Within a certain spatial region, distributed electrical devices (nodes) establish virtual power channels based on WPT technology, forming a localized WPTN. Nodes in this network can flexibly switch among several functional roles according to demand, including power transmitting nodes, relay nodes, and power receiving nodes. Specifically, power transmitting nodes supply energy to other nodes, relay nodes primarily extend the power transmission distance between nodes, and power receiving nodes correspond to devices requiring energy intake. When a node exits the power transmission network, it can switch to a decoupled state, where it is open circuit in the power transfer network through switches, resulting in negligible mutual inductance coupling with other active nodes and near-zero coil current.

For example, the cluster charging method in AGV systems in factories as illustrated in Fig. 1, can be considered a small-scale localized WPTN. Based on preset power transmission rules and considering the actual energy requirements and task priorities of individual AGVs, efficient energy allocation can be achieved. Within this architecture, each node can flexibly alter its functional role as needed, and nodes not participating in the current power transfer remain in a decoupled state. Such a

Fig. 1. AGV-based localized WPTN.

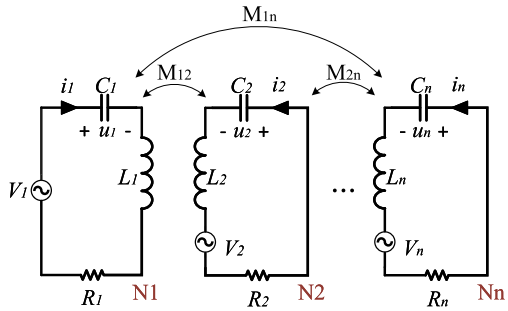

Fig. 2. Equivalent circuit of a WPTN.

WPT-based adaptive network architecture provides an efficient energy management solution for mobile equipment in smart factories.

The WPTN system consists of multiple transmitting, relay, and receiving coils, and its equivalent circuit is shown in Fig. 2. Parameters for each circuit node include load R_L and equivalent internal resistance R_n, coil self-inductance L_n, compensation capacitance C_n, voltage across the compensation capacitor u_n, coil current i_n, and source voltage V_n. The coupling coefficient between the ith and jth coils is represented by $M_{ij}(i \neq j)$. In existing studies, cross-coupling between nonadjacent coils is often neglected in multinode WPT systems. However, in practical applications, the impact of cross-coupling cannot be overlooked due to typically unknown node quantities and spatial configurations. Particularly in power transfer network with numerous and complexly structured nodes, cross-coupling effects may significantly influence system performance. Thus, cross-coupling effects must be adequately considered during WPTN modeling and analysis to ensure accuracy.

Taking cross-coupling into account, the mathematical model for the WPTN system depicted in Fig. 2 can be established based on Kirchhoff's Voltage Law (KVL), as shown follows:

$$\begin{cases} L_1C_1\ddot{u}_1 + \sum_{k\neq 1} M_{1k}C_k\ddot{u}_k + R_1C_1\dot{u}_1 + u_1 = V_1 \\ L_2C_2\ddot{u}_2 + \sum_{k\neq 2} M_{2k}C_k\ddot{u}_k + R_2C_2\dot{u}_2 + u_2 = V_2 \\ \quad \vdots \\ L_nC_n\ddot{u}_n + \sum_{k\neq n} M_{nk}C_k\ddot{u}_k + R_nC_n\dot{u}_n + u_n = V_n. \end{cases} \tag{1}$$

The mathematical model in (1) adopts the Fundamental Harmonic Approximation (FHA), retaining only the fundamental frequency components. This is justified for high-Q resonant WPTN systems, where resonant tanks effectively filter out higher-order harmonics, as supported by both theory and experimental results [31].

Define vector $\mathbf{V}$ as the source voltage, $\mathbf{i}$ as resonant current, and $\mathbf{u}$ as capacitor voltage. The matrices $\mathbf{L}$,$\mathbf{C}$, and $\mathbf{R}$ represent the system inductance, capacitance, and resistance matrices, respectively, expressed as follows:

$$\mathbf{V} = \begin{bmatrix} V_1 \\ V_2 \\ \vdots \\ V_n \end{bmatrix}, \mathbf{i} = \begin{bmatrix} i_1 \\ i_2 \\ \vdots \\ i_n \end{bmatrix}, \mathbf{u} = \begin{bmatrix} u_1 \\ u_2 \\ \vdots \\ u_n \end{bmatrix} \tag{2}$$

$$\mathbf{L} = \begin{bmatrix} L_1 & M_{12} & \cdots & M_{1n} \\ M_{21} & L_2 & \cdots & M_{2n} \\ \vdots & \vdots & \ddots & \vdots \\ M_{n1} & M_{n2} & \cdots & L_n \end{bmatrix}$$

$$\mathbf{C} = \begin{bmatrix} C_1 & 0 & \cdots & 0 \\ 0 & C_2 & \cdots & 0 \\ \vdots & \vdots & \ddots & \vdots \\ 0 & 0 & \cdots & C_n \end{bmatrix}$$

$$\mathbf{R} = \begin{bmatrix} R_1 & 0 & \cdots & 0 \\ 0 & R_2 & \cdots & 0 \\ \vdots & \vdots & \ddots & \vdots \\ 0 & 0 & \cdots & R_n \end{bmatrix}. \tag{3}$$

According to [32], the current at each node can be expressed as follows:

$$i_{pi} = \left| \left(-\omega^2\mathbf{LC} + j\omega\mathbf{RC} + \mathbf{I}\right)^{-1} \omega C_i \mathbf{V} \right| \tag{4}$$

where $\mathbf{I}$ is the identity matrix, C_i represents the compensation capacitor of the ith node as an element of matrix $\mathbf{C}$, and mutual inductances between nodes i and j satisfy $M_{ij} = M_{ji}$. It can be seen from (1) that when the dimensionality of unknown mutual inductances $M(\dim(M) = n)$exceeds the number of equations (i.e.,$n > m$), the system becomes underdetermined. In this case, it is impossible to analytically solve the system and directly obtain the values of M in matrix $\mathbf{L}$.

B. Power and Efficiency Model for WPTN Paths

In the AGV WPTN, the dynamic access and exit of nodes (such as the addition of new AGVs or node departure due to task scheduling) cause real-time changes in the network topology. These dynamic topology changes lead to the reconstruction of coupling relationships in power transfer paths, resulting in voltage fluctuations and power oscillations in the system, which in turn affect the power transfer efficiency of the system. Therefore, to achieve real-time path switching and maintain system stability, it is necessary to calculate the transmission power and efficiency of different paths in real-time to determine the optimal power transfer path.

According to the node current expression (4), when all mutual inductance parameters in the power transfer network are known, the power and efficiency of each transmission path can be calculated using the updated coupling matrix. Specifically, the input power P_{in}, output power P_{out}, and efficiency η_k of the transmission path are defined by the following formulas:

$$P_{\text{in}} = V_{\text{in}} i_{\text{in}} = f_1(V_{\text{in}}, R_{\text{eq}}) \tag{5}$$

$$P_{\text{out}} = i_{\text{out}}^2 R_{\text{eq}} = f_2(V_{\text{in}}, R_{\text{eq}}) \tag{6}$$

$$\eta_k = \frac{P_{\text{out},k}}{P_{\text{in},k}} = \frac{f_2(V_{\text{in}}, R_{\text{eq}})}{f_1(V_{\text{in}}, R_{\text{eq}})}, \quad k = 1, 2, \ldots, n. \tag{7}$$

In this context, V_{in} represents the input voltage, R_{eq} denotes the equivalent load, and i_{pi} is the node current. To maximize transmission efficiency while meeting power requirements, the system adjusts the input voltage via a dc–dc converter and controls the equivalent load by adjusting the phase shift angle. To determine the optimal values of these parameters, the following dual-constraint optimization problem is established:

$$\max_{V_{\text{in}}, R_{\text{eq}}} \eta_k$$
$$s.t. \begin{cases} P_k(V_{\text{in}}, R_{\text{eq}}) \geq P_{\min} \\ 0 < V_{\text{in}} \leq V_{\max} \\ 0 < R_{\text{eq}} \leq R_{\max} \end{cases}. \tag{8}$$

In this context, $P_{\min}$ represents the minimum power requirement of the system. Due to the highly nonlinear nature of the optimization problem (8), traditional numerical methods are difficult to apply directly. Therefore, this article employs a quadtree spatial search algorithm. This algorithm is based on the divide-and-conquer strategy of binary trees and achieves efficient searching by recursively partitioning the 2-D parameter space. Within the parameter space $0 < V_{\text{in}} \leq V_{\max}$ and $0 < R_{\text{eq}} \leq R_{\max}$, the entire region is set as the root node, and the execution process is illustrated in Fig. 3.

The algorithm execution process follows a three-level pruning strategy: 1) Power constraint pruning: Calculate the power P_{k} at the center point of the sub-region, and prune if $P_{\text{k}} < P_{\min}$. 2) Efficiency boundary pruning: Calculate the maximum possible efficiency $\eta_k^{\max}$ at the vertices of the region, and prune if $\eta_k^{\max} < \eta_{\text{current}}^{\text{best}}$ ($\eta_{\text{current}}^{\text{best}}$ represents the best efficiency value found during the current search process). 3) Parameter boundary pruning: Exclude regions that exceed the constraints of $V_{\max}/R_{\max}$. As shown in the figure, the algorithm recursively partitions the parameter space and applies pruning strategies. It terminates when the region size meets the accuracy requirements and selects the center point with the largest η_k from the unpruned regions as the optimal solution.

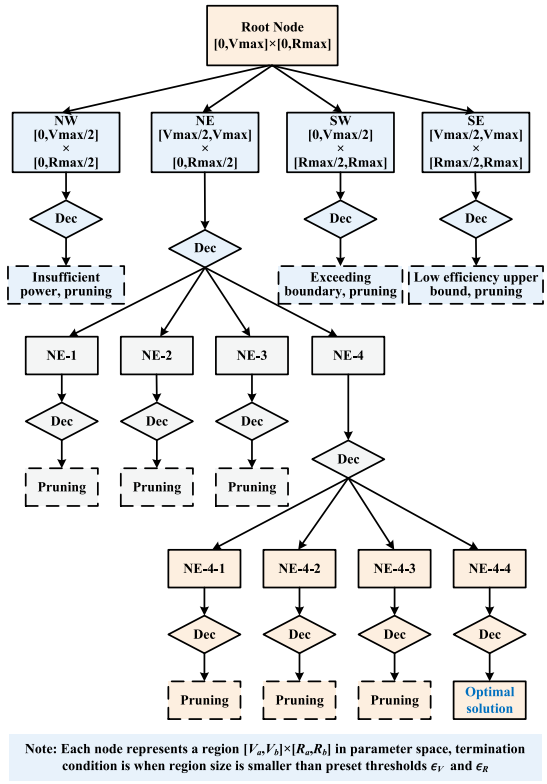

Fig. 3. Execution process of the quadtree optimization algorithm.

III. Gradient Descent Based on Backpropagation

A. Mutual Inductance Identification Procedure

Based on the previous analysis, an explicit analytical expression for the mutual inductance in WPTN cannot be obtained. Therefore, this article establishes a numerical solution framework based on gradient descent, with the core idea of transforming the mutual inductance identification into a nonlinear optimization problem subject to physical constraints

$$\min_M \mathcal{L}(M) = \frac{1}{2} \left\| \left| \text{inv}\left(-\omega^2 \mathbf{LC} + j\omega \mathbf{RC} + \mathbf{I}\right) \omega C_i \mathbf{V} \right| - \ i_i \right\|_2^2$$
$$\text{s.t.} \quad M \in \mathcal{D}_{\text{phys}} \tag{9}$$

where i_i represents the coil current measured in practice. The gradient descent algorithm is used to generate an iterative sequence $M^0, M^1, M^2, \ldots$ ensuring $\mathcal{L}(M^{k+1}) < \mathcal{L}(M^k)$ at each iteration. The iterative update rule is as follows:

$$M^{k+1} = \text{Proj}_{\mathcal{D}_{\text{phys}}} \left(M^k - \eta_k \nabla \mathcal{L}(M^k) \right). \tag{10}$$

To improve convergence efficiency, the Adam optimizer is introduced to update gradient direction and step size. The Adam optimizer is well-suited for this multiparameter identification problem, which is crucial for real-time applications in dynamic WPTN environments. The Adam update rules are as follows:

$$m^{k+1} = \beta_1 m^k + (1 - \beta_1) \nabla \mathcal{L}$$
$$v^{k+1} = \beta_2 v^k + (1 - \beta_2) (\nabla \mathcal{L})^2$$
$$\hat{m}^{k+1} = \frac{m^{k+1}}{1 - \beta_1^{k+1}}$$
$$\hat{v}^{k+1} = \frac{v^{k+1}}{1 - \beta_2^{k+1}}$$

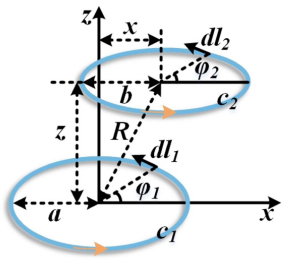

Fig. 4. Geometric configuration of current-carrying conductors for mutual inductance calculation using Neumann formula.

$$M_{\text{temp}}^{k+1} = M^k - \frac{\eta_k \hat{m}^{k+1}}{\sqrt{\hat{v}^{k+1}} + \epsilon}. \tag{11}$$

The learning rate η_k adopts a combined strategy of StepLR and CosineAnnealingLR, satisfying the convergence conditions $\sum \eta_k = +\infty$ and $\sum \eta_k^2 < +\infty$.

To enhance mutual inductance prediction accuracy, mutual inductance constraints based on Neumann's formula are introduced. As shown in Fig. 4, geometric parameters of two current-carrying conductors—including radii a, b, axial distance R, vertical spacing z, lateral offset x, and horizontal offset angles φ_1, φ_2—determine the theoretical range of mutual inductance According to [33] and [34] and Maxwell's equations, the mutual inductance between coils is given by

$$M_{ij} = \frac{\mu_0}{4\pi} \int_{c_1} \int_{c_2} \frac{1}{R}\, d\vec{l_1} \cdot d\vec{l_2} \tag{12}$$

where the distance R can be expressed as

$$R = \sqrt{\begin{matrix} a^2 + b^2 + z^2 + x^2 - 2ab\cos(\varphi_1 - \varphi_2) \\ + 2xb\cos\varphi_2 - 2xa\cos\varphi_1. \end{matrix}} \tag{13}$$

For practical multiturn coils, the total mutual inductance between the primary coil with n_p turns and the secondary coil with n_s turns is represented as a linear superposition of single-turn mutual inductances

$$M = \rho \times \sum_{i=1}^{n_p} \sum_{j=1}^{n_s} M_{ij}. \tag{14}$$

Here, μ_0 is the vacuum permeability, M_{ij} is the mutual inductance between single-turn conductors c_1 and c_2, and $\rho \in (0, 1)$ is the coil shape correction factor. In WPTN, node geometry parameters (a, b, z, x, φ) are constrained by physical layouts. According to (14), the theoretical boundaries of mutual inductance between any two nodes can be derived

$$\mathcal{D}_{\text{phys}} = \left\{ M_{ij} \in \mathbb{R}^+ \,\middle|\, M_{ij}^{\min} \le M_{ij} \le M_{ij}^{\max} \right\}. \tag{15}$$

Algorithm 1 describes the proposed algorithm, including gradient calculation, Adam updates, physical constraint projection, and learning rate adjustments.

To validate the algorithm's effectiveness, a four-node WPTN simulation platform was established with randomly generated operating conditions. System parameters are presented in Table I.

TABLE I
FOUR-NODE SYSTEM SIMULATION PARAMETERS

V_{in}	0∼20 V	f	150∼600 kHz
L_1, L_2, L_3, L_4	100 μH	R_L	1∼10 Ω
M_{12}, M_{13}, M_{23}	0∼20 μH	M_{23}, M_{24}, M_{34}	0∼20 μH

Algorithm 1: Gradient Descent-Based Mutual Inductance Parameter Identification Algorithm.

Initialization: Mutual inductance parameters $M^0 \sim \mathcal{U}(M_{\min}, M_{\max})$, learning rate $\eta_0 = 0.001$, maximum iterations $K_{\max} = 5,000$, stopping threshold $\epsilon = 1e-4$, momentum parameters $\beta_1 = 0.9, \beta_2 = 0.999$, first moment $m^0 = 0$, second moment $v^0 = 0$, optimal solution $M_{\text{best}} = M^0$, $\mathcal{L}_{\text{best}} = \mathcal{L}(M^0)$
Compute initial gradient $\nabla\mathcal{L}(M^0)$: $\nabla\mathcal{L} = 2\frac{\partial \mathcal{L}}{\partial M^*}$ ▷Wirtinger derivative
for $k = 1, \ldots, K_{\max}$ **do**
  Compute gradient norm: $\epsilon_k = \|\nabla\mathcal{L}(M^{k-1})\|_2$
  if $\epsilon_k < \epsilon$ **or** $\frac{|\mathcal{L}(M^{k-1}) - \mathcal{L}(M^{k-2})|}{\mathcal{L}(M^{k-2})} < 1e-4$ **then**
    break
  end if
  Vanilla Update: $M_{\text{temp}} = M^{k-1} - \eta_0 \nabla\mathcal{L}(M^{k-1})$
  if $k \bmod 500 = 0$ **or** $|\mathcal{L}(M^{k-1}) - \mathcal{L}(M^{k-2})| < 1e-5 \cdot \mathcal{L}(M^{k-2})$ **then**
    Update first moment: $m^k = \beta_1\, m^{k-1} + (1-\beta_1)\nabla\mathcal{L}$
    Update second moment: $v^k = \beta_2 v^{k-1} + (1-\beta_2)(\nabla\mathcal{L})^2$
    Bias correction: $\hat{m}^k = m^k/(1-\beta_1^k)$
    Bias correction: $\hat{v}^k = v^k/(1-\beta_2^k)$
    Adam update: $M_{\text{temp}} = M^{k-1} - \eta_k \hat{m}^k/(\sqrt{\hat{v}^k} + \epsilon)$
  end if
  Projection onto feasible domain: $M^k = \max(M_{\min}, \min(M_{\max}, M_{\text{temp}}))$
  Update learning rate: $\eta_k = 0.7^{\lfloor k/1000 \rfloor} \cdot \eta_0 \cdot \frac{1}{2}(1 + \cos(\pi k/K_{\max}))$
  if $\mathcal{L}(M^k) < \mathcal{L}_{\text{best}}$ **then**
    Update optimal solution: $M_{\text{best}} = M^k$, $\mathcal{L}_{\text{best}} = \mathcal{L}(M^k)$
  end if
end for
Return: M_{best}

Results show that all relative errors were below 7%, with average errors of mutual inductances M_{14}, M_{24}, and M_{34} being 1.3%, 1.6%, and 1.4%, respectively, and their corresponding maximum errors being 4.68%, 5.16%, and 4.49%, respectively. Fig. 5 compares the identified and actual mutual inductances for 50 randomly selected samples. Fig. 6 further illustrates the error distribution of these 50 sets of data, demonstrating algorithm stability.

Fig. 7 records the optimization trajectory of the loss function, indicating stable convergence to a global optimum without local stagnation.

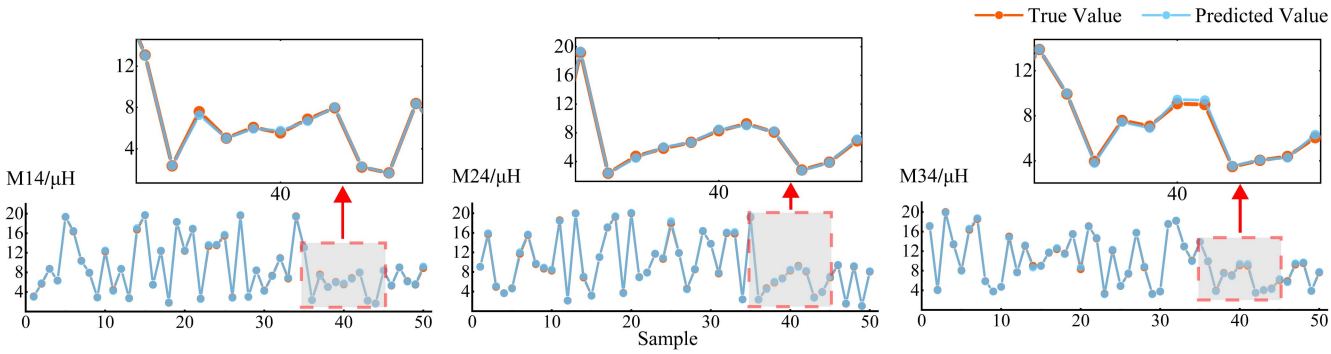

Fig. 5. Comparison between identified and actual mutual inductance values.

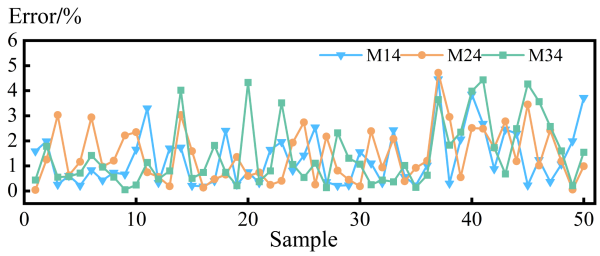

Fig. 6. Relative error distribution of mutual inductance identification results.

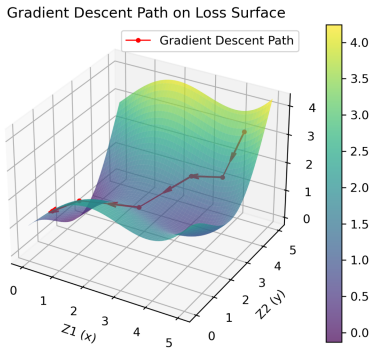

Fig. 7. Gradient descent trajectory.

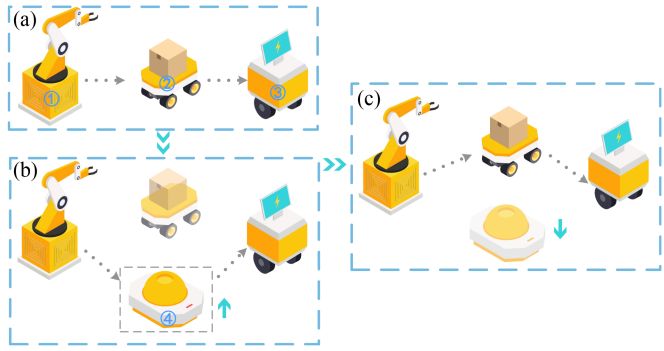

Fig. 8. Dynamic node update process.

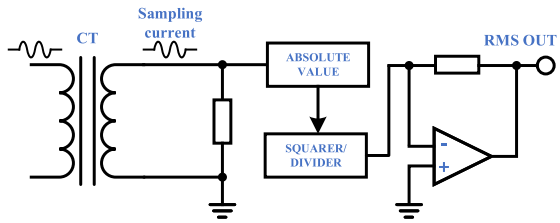

Fig. 9. AD637 sampling circuit.

B. Path Optimization Procedure

When nodes in the WPTN change dynamically, such as new nodes joining or existing nodes leaving, the system must dynamically update the power transfer path. Taking a three-node system as an example, assume node 1 is the transmitter and node 3 is the receiver. After a new node AGV4 joins the system, the network configuration updates as shown in Fig. 8:

Based on the previously described mutual inductance identification method, the updated coupling matrix L_{NEW} can be obtained, where the mutual inductances associated with the newly added node and the original system are marked in blue:

$$L_{\text{NEW}} = \begin{bmatrix} L_1 & M_{12} & M_{13} & M_{14} \\ M_{21} & L_2 & M_{23} & M_{24} \\ M_{31} & M_{32} & L_3 & M_{34} \\ M_{41} & M_{42} & M_{43} & L_4 \end{bmatrix}. \tag{16}$$

At this point, the power transfer network has three candidate paths

1) *Path 1*: $1 \rightarrow 2 \rightarrow 3$
2) *Path 2*: $1 \rightarrow 4 \rightarrow 3$
3) *Path 3*: $1 \rightarrow 24 \rightarrow 3$

To achieve dynamic path optimization for power transfer, this article integrates Bluetooth modules in each node circuit. Coil current signals at each node are collected in real-time using the AD637 module, which performs hardware-based true RMS conversion through continuous analog computation, as illustrated in Fig. 9, and transmitted synchronously to a computer or processor.

Based on the updated coupling matrix, the power transfer efficiency and transmitted power for each candidate path can be calculated using (6) and (7), respectively. Subsequently, the control terminal determines the optimal path that meets the power demand with the highest transfer efficiency. Once the

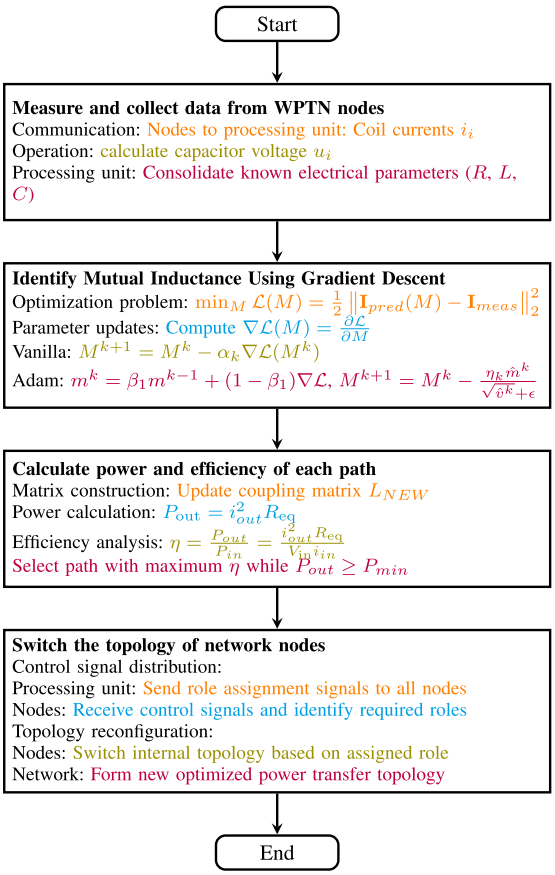

Fig. 10. WPTN mutual inductance identification and path optimization flowchart.

TABLE II
EXPERIMENTAL SYSTEM PARAMETER CONFIGURATION

V_{in}	0∼100 V	f	475 kHz
L_1	37.7 μH	C_1, C_2, C_3, C_4	3.26 nF
L_2	36.3 μH	R_1, R_2, R_3, R_4	0.26 Ω
L_3	35.5 μH	R_L	50 Ω
L_4	37 μH		

TABLE III
COIL CURRENT MEASUREMENTS UPON NODE INTRODUCTION AT DIFFERENT POSITIONS (A)

Group	i_1	i_2	i_3	i_4
1	2.9	4.3	2.2	2.6
2	3.6	6.6	2.1	2.1
3	3.7	4	2.8	2

optimal path is identified, the control terminal assigns roles to each node (transmitter, relay node, or decoupled state) according to the optimization result and transmits this role information via Bluetooth to the microcontrollers in each node, driving the nodes to switch their circuit topology accordingly. Fig. 10 illustrates the mutual inductance identification and dynamic path optimization process for the WPTN.

After completing the path optimization decision, nodes not involved in power transfer (e.g., AGV2) switch to a decoupled state via FET switches, while relay nodes (e.g., AGV4) remain in

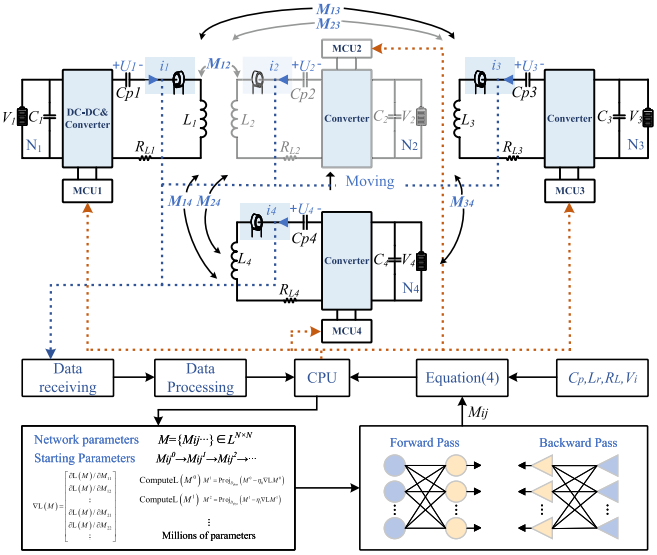

Fig. 11. Control schematic diagram.

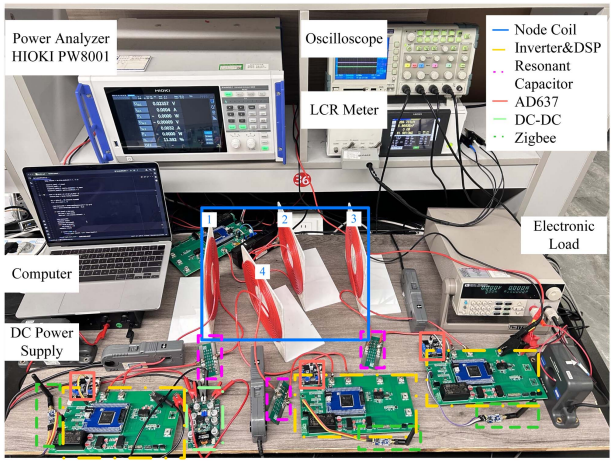

Fig. 12. Four-node WPTN experimental platform.

resonance. When AGV4 leaves the network, the system triggers a path rollback mechanism. AGV2 switches from the decoupled state back to a relay state, reverting the power transfer path to the original Path 1 (1→ 2→ 3), and AGV3 maintains a constant power charging mode through impedance matching during the switching process. This control strategy effectively ensures continuous power transmission during node dynamic changes. Fig. 11 shows the control block diagram for the described system.

IV. EXPERIMENT

To validate the effectiveness of the proposed mutual inductance identification method, a four-node WPTN experimental platform was constructed, as shown in Fig. 12, with system parameters provided in Table II.

Three sets of experiments were designed to simulate the scenario where node 4 is introduced at different spatial positions. Initial coupling matrices (unit: μH) for nodes 1–3 in each

TABLE IV
WAVEFORMS OF PATH SWITCHING EXPERIMENTS

	Path 123	Path 143	Path $1^2$43	Switching Process	Node Position
Case1	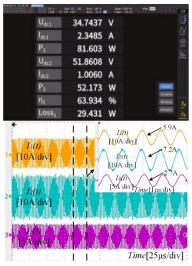	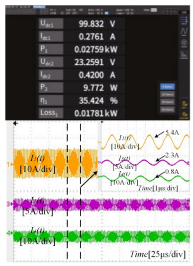	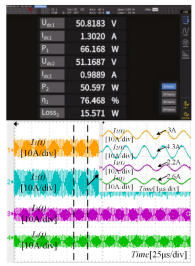	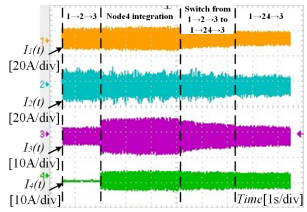	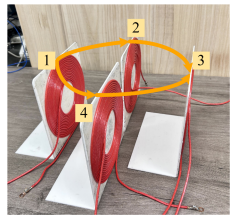
Case2	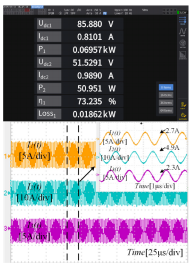	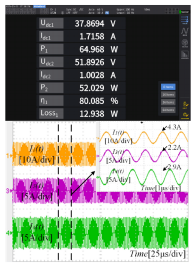	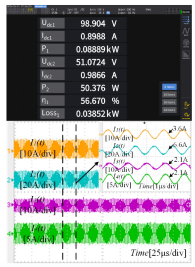	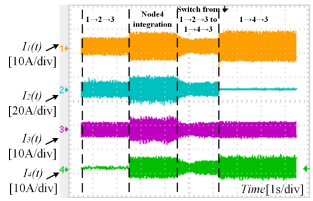	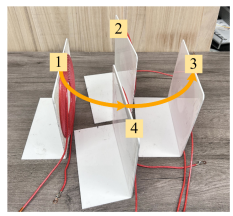
Case3	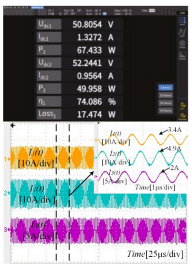	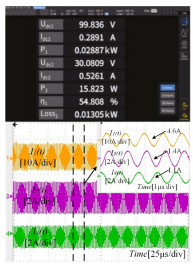	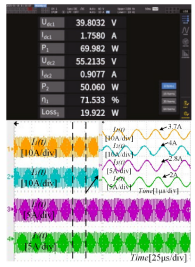	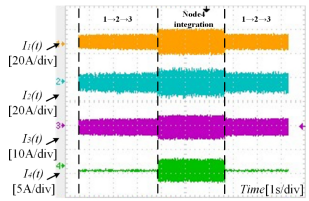	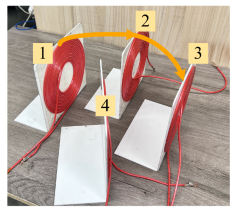

experimental scenario are shown as follows:

$$L_1 = \begin{bmatrix} 37.7 & 2.44 & 1.1 \\ 2.44 & 36.3 & 1.9 \\ 1.1 & 1.9 & 35.5 \end{bmatrix}$$

$$L_2 = \begin{bmatrix} 37.7 & 4.1 & 1.82 \\ 4.1 & 36.3 & 2.4 \\ 1.82 & 2.4 & 35.5 \end{bmatrix}$$

$$L_3 = \begin{bmatrix} 37.7 & 3.22 & 1.23 \\ 3.22 & 36.3 & 2.74 \\ 1.23 & 2.74 & 35.5 \end{bmatrix}. \quad (17)$$

When node 4 is introduced, measured coil currents at each node are collected as shown in Table III, and transmitted to a host computer via Bluetooth for mutual inductance parameter identification.

Based on these currents, Table V compares measured and identified mutual inductance parameters. Results indicate a maximum relative error of 5.83%, with an average error of 4.77% across multiple identifications, validating the effectiveness of the proposed algorithm.

Based on the updated coupling matrix, the transmission efficiency η and output power P_{out} for each optimal path are calculated. Table VI shows the calculated transmitted power and efficiency for each path under input voltages within 100 V.

TABLE V
COMPARISON OF MEASURED AND IDENTIFIED MUTUAL INDUCTANCE PARAMETERS ACROSS DIFFERENT EXPERIMENTAL GROUPS

Group	Parameters	Measured Values	Estimation Values	Errors
1	M_{14}	1.1 μH	1.1571 μH	5.19%
	M_{24}	−1 μH	−1.0389 μH	3.89%
	M_{34}	1 μH	1.0562 μH	5.62%
2	M_{14}	3.4 μH	3.5527 μH	4.5%
	M_{24}	1.2 μH	1.2667 μH	5.6%
	M_{34}	4.43 μH	4.2961 μH	3%
3	M_{14}	0.3 μH	0.2839 μH	5.37%
	M_{24}	0.48 μH	0.452 μH	5.83%
	M_{34}	1.78 μH	1.7094 μH	3.97%

Table IV presents the key waveforms of node currents during path switching, along with corresponding receiver power and efficiency. Three scenarios at different node positions were selected, each including three transfer paths: path① (1→ 2→ 3), path② (1→ 4→ 3), and path③ (1→^{2} 4 → 3).

1) *Case 1*: Path① dc output voltage is 35 V, node 3 power is 52 W, efficiency is 64%; Path② dc output voltage is 100 V, but node 3 power does not reach 50 W; Path③ dc

TABLE VI
COMPARISON OF POWER AND EFFICIENCY ACROSS THREE TRANSMISSION PATHS IN DIFFERENT EXPERIMENTAL GROUPS

Group	Path	Performance Metrics	
		Power(W)	Efficiency (%)
1	123	60	71.2
	143	7.8	44.8
	$1^2$43	50	84.4
2	123	52	84
	143	55	87
	$1^2$43	55	76
3	123	57	85.1
	143	19	75
	$1^2$43	58	83

output voltage is 51 V, node 3 power is 51 W, efficiency is 76.5%.

2) *Case 2*: Path① dc output voltage is 86 V, node 3 power is 52 W, efficiency is 73.2%; Path② dc output voltage is 38 V, node 3 power is 55 W, efficiency is 80%; Path③ dc output voltage is 99 V, node 3 power is 55 W, efficiency is 56.7%.
3) *Case 3*: Path① dc output voltage is 51 V, node 3 power is 50 W, efficiency is 74.1%; Path② dc output voltage is 100 V, but node 3 power does not reach 50 W; Path③ dc output voltage is 40 V, node 3 power is 50 W, efficiency is 71.5%.

By calculating the power and transmission efficiency along different paths, the accuracy of the identified mutual inductance and the feasibility of path optimization are further verified. Observations indicate that the path switching process is relatively smooth, with no significant fluctuations. The experiments show an average difference of about 10% between the measured efficiencies and the theoretical predictions, primarily due to losses in the power converter. These results further validate the accuracy of the proposed mutual inductance identification method.

V. DISCUSSION

This article provides an effective solution for mutual inductances identification in dynamically reconfigurable WPTN, broadening the application scope of WPTN systems. Future research could explore the following directions:

A. Extended Application to Dynamic Scenarios

To extend the proposed method to continuous movement scenarios where AGVs are in motion, a dual-mode hybrid control framework could be developed: employing high-precision identification during stationary periods and switching to fast power regulation control during motion, where mutual inductance variations are treated as disturbances to be compensated by real-time power electronics control. This approach would enable the system to maintain stable power delivery while accommodating the dynamic nature of mobile AGV applications.

B. Applicability to Different WPTN Topologies

The effectiveness of our proposed mutual inductance identification method is fundamentally dependent on the accuracy of the underlying WPTN mathematical model. As long as a sufficiently precise mathematical model can be established for any specific compensation topology, our gradient descent-based identification approach remains applicable.

C. Multi-Parameter Identification Capability

The current model focuses primarily on mutual inductance identification while treating other system parameters as known. However, the gradient descent framework naturally extends to simultaneous identification of multiple parameters, including load resistance, capacitance variations, and frequency shifts. Future work will explore comprehensive multiparameter identification to enhance system adaptability under diverse operating conditions, particularly for industrial applications requiring real-time adaptation to multiple varying parameters.

VI. CONCLUSION

This article proposed a dynamic mutual inductance identification method based on the gradient descent algorithm. By monitoring the coil currents of nodes in the WPTN in real time, the coupling parameter matrix can be dynamically updated when node changes occur, either in position or quantity. This effectively addresses the challenge of synchronous identification of multiple mutual inductance parameters caused by network topology changes in WPTN. The main advantages of the proposed method are as follows: 1) The proposed method enables real-time tracking of dynamic topology variations and synchronous identification of multiple coupled mutual inductances, overcoming the limitations of traditional methods in complex network topologies. 2) Based on the dynamically identified coupling parameters, an efficiency-oriented transmission path optimization strategy is developed, which allows for dynamic adjustment of network topology and optimal path reconstruction. This approach maximizes system power transfer efficiency while ensuring power supply stability. Overall, the proposed method breaks through the limitations of traditional methods, providing a new approach for mutual inductance identification and path optimization in WPTN systems with any number of nodes.

REFERENCES

[1] C. Y. Xia et al., "Inductive power transfer system for tail-free household appliances in smart home system," *IET Power Electron.*, vol. 12, no. 5, pp. 1002–1010, 2019.
[2] W. Zhou, Y.-G. Su, L. Huang, X.-D. Qing, and A. P. Hu, "Wireless power transfer across a metal barrier by combined capacitive and inductive coupling," *IEEE Trans. Ind. Electron.*, vol. 66, no. 5, pp. 4031–4041, May 2019.
[3] J. Zhou, B. Zhang, W. Xiao, D. Qiu, and Y. Chen, "Nonlinear parity-time-symmetric model for constant efficiency wireless power transfer: Application to a drone-in-flight wireless charging platform," *IEEE Trans. Ind. Electron.*, vol. 66, no. 5, pp. 4097–4107, May 2019.

[4] R. Xie et al., "A simple integrated solution of reconfigurable wired and wireless vehicle-to-vehicle (V2V) charging system," *Wireless Power Transfer*, vol. 11, 2024, Art. no. wpt-0024-0013, doi: 10.48130/wpt-0024-0013.
[5] Y. Feng, Y. Sun, T. Lin, H. Hu, and F. Chen, "Mutual inductance surrogate model of the UWPT system and its constant power optimization at misaligned positions," *Wireless Power Transfer*, vol. 11, 2024, Art. no. wpt-0024-0001, doi: 10.48130/wpt-0024-0001.
[6] U. K. Madawala and D. J. Thrimawithana, "A bidirectional inductive power interface for electric vehicles in V2G systems," *IEEE Trans. Ind. Electron.*, vol. 58, no. 10, pp. 4789–4796, Oct. 2011.
[7] U. K. Madawala and D. J. Thrimawithana, "Modular-based inductive power transfer system for high-power applications," *IET Power Electron.*, vol. 5, no. 7, pp. 1119–1126, Jul. 2012.
[8] A. K. Swain, S. Devarakonda, and U. K. Madawala, "Modeling, sensitivity analysis, and controller synthesis of multipickup bidirectional inductive power transfer systems," *IEEE Trans. Ind. Informat.*, vol. 10, no. 2, pp. 1372–1380, May 2014.
[9] J. Wu, X. Dai, Y. Sun, and Y. Li, "A node role dynamic change method among repeater, receiver, and decoupling using topology switching in multinode WPT system," *IEEE Trans. Power Electron.*, vol. 36, no. 10, pp. 11174–11182, Oct. 2021, doi: 10.1109/TPEL.2021.3072203.
[10] J. Wu, Y. Li, X. Dai, R. Gao, and M. He, "A dynamic power transfer route construction and optimization method considering random node distribution for wireless power transfer network," *IEEE Trans. Power Electron.*, vol. 39, no. 4, pp. 4858–4869, Apr. 2024, doi: 10.1109/TPEL.2023.3348103.
[11] S. S. H. Yazdi, A. Namadmalan, A. Kapanov, A. Zollanvari, and M. Bagheri, "Optimal design of D-IPT systems considering mutual inductances and number and location of repeaters," in *Proc. IEEE Int. Conf. Environ. Elect. Eng. IEEE Ind. Commercial Power Syst. Europe*, 2022, pp. 1–6.
[12] J.-H. Cho, S. Jung, and Y.-J. Kim, "Wireless power transfer for variable load, distance, and power division ratio in a loosely-coupled multiple-receiver relay system," *IEEE Trans. Ind. Electron.*, vol. 70, no. 7, pp. 6809–6818, Jul. 2022.
[13] J. Wu, Z. Jin, X. Han, W. Zhang, Q. Zhao, and Z. Liang, "Construction and optimization of power transfer route in array wireless power transfer network with multiple load nodes," *IEEE Trans. Power Electron.*, vol. 39, no. 3, pp. 3842–3850, Mar. 2024, doi: 10.1109/TPEL.2023.3339974.
[14] X. Dai, X. Li, Y. Li, and A. P. Hu, "Maximum efficiency tracking for wireless power transfer systems with dynamic coupling coefficient estimation," *IEEE Trans. Power Electron.*, vol. 33, no. 6, pp. 5005–5015, Jun. 2018.
[15] L. Wang et al., "Mutual inductance identification of IPT system based on soft-start process," *IEEE Trans. Power Electron.*, vol. 37, no. 6, pp. 7504–7517, Jun. 2022, doi: 10.1109/TPEL.2022.3142289.
[16] J. Hu, J. Zhao, and C. Cui, "A wide charging range wireless power transfer control system with harmonic current to estimate the coupling coefficient," *IEEE Trans. Power Electron.*, vol. 36, no. 5, pp. 5082–5094, May 2021.
[17] J. Zeng, Y. Yang, K. Li, S. Chen, and S. Y. R. Hui, "An ultrafast estimation method for coupling coefficient and receiver resonant frequency in universal wireless power transfer systems," *IEEE Trans. Power Electron.*, vol. 39, no. 4, pp. 4870–4883, Apr. 2024, doi: 10.1109/TPEL.2023.3348453.
[18] K. Yue, Y. Liu, P. Zhao, B. Xue, and R. He, "Time domain coupling coefficient estimation using transmitter-side information in wireless power transfer system," in *Proc. 45th Annu. Conf. IEEE Ind. Electron. Soc.*, Oct. 2019, pp. 4189–4194.
[19] Y. Su, L. Chen, X.-Y. Wu, A. P. Hu, C.-S. Tang, and X. Dai, "Load and mutual inductance identification from the primary side of inductive power transfer system with parallel-tuned secondary power pickup," *IEEE Trans. Power Electron.*, vol. 33, no. 11, pp. 9952–9962, Nov. 2018.
[20] J. Liu, G. Wang, G. Xu, J. Peng, and H. Jiang, "A parameter identification approach with primary-side measurement for DC–DC wireless-power-transfer converters with different resonant tank topologies," *IEEE Trans. Transp. Electrific.*, vol. 7, no. 3, pp. 1219–1235, Sep. 2021.
[21] L. Wang et al., "Joint real-time identification for mutual inductance and load charging parameters of IPT system," *IEEE J. Emerg. Sel. Topics Power Electron.*, vol. 11, no. 4, pp. 4574–4590, Aug. 2023.
[22] Y. Liu and H. Feng, "Maximum efficiency tracking control method for WPT system based on dynamic coupling coefficient identification and impedance matching network," *IEEE J. Emerg. Sel. Topics Power Electron.*, vol. 8, no. 4, pp. 3633–3643, Dec. 2020.
[23] X. Sheng and L. Shi, "Mutual inductance and load identification method for inductively coupled power transfer system based on auxiliary inverter," *IEEE Trans. Veh. Technol.*, vol. 69, no. 2, pp. 1533–1541, Feb. 2020.
[24] Y. Yang, S. C. Tan, and S. Y. R. Hui, "Fast hardware approach to determining mutual coupling of series–series-compensated wireless power transfer systems with active rectifiers," *IEEE Trans. Power Electron.*, vol. 35, no. 10, pp. 11026–11038, Oct. 2020, doi: 10.1109/TPEL.2020.2977140.
[25] K. Yue, Y. Liu, X. Zhang, R. He, and M. Fu, "Identifying complete set of parameters using transmitter side information for multi-transmitter wireless power transfer systems," in *Proc. IEEE Appl. Power Electron. Conf. Expo.*, 2022, pp. 1128–1132.
[26] X. Liu, D. Jin, H. Ji, L. Liu, and C. Xia, "Research on mutual inductance identification and efficiency optimization of the three-coil wireless power transfer systems with switchable relay coil," *IEEE Trans. Power Electron.*, vol. 39, no. 5, pp. 6492–6503, May 2024, doi: 10.1109/TPEL.2024.3363138.
[27] Y. Yang, S.-C. Tan, and S. Y. R. Hui, "Front-end parameter monitoring method based on two-layer adaptive differential evolution for SS-Compensated wireless power transfer systems," *IEEE Trans. Ind. Informat.*, vol. 15, no. 11, pp. 6101–6113, Nov. 2019, doi: 10.1109/TII.2019.2924926.
[28] D.-H. Kim, S. Kim, S.-W. Kim, J. Moon, I. Cho, and D. Ahn, "Coupling extraction and maximum efficiency tracking for multiple concurrent transmitters in dynamic wireless charging," *IEEE Trans. Power Electron.*, vol. 35, no. 8, pp. 7853–7862, Aug. 2020.
[29] D.-H. Kim and D. Ahn, "Maximum efficiency point tracking for multiple-transmitter wireless power transfer," *IEEE Trans. Power Electron.*, vol. 35, no. 11, pp. 11391–11400, Nov. 2020, doi: 10.1109/TPEL.2019.2919293.
[30] C. Zhu, J. Ren, and W. Zhong, "Phase-identification-based mutual inductance estimation methodology for modular wireless power transfer systems," *IEEE Trans. Transp. Electrific.*, vol. 11, no. 2, pp. 5211–5222, Apr. 2025, doi: 10.1109/TTE.2024.3477412.
[31] Z.-J. Liao, Y. Sun, Z.-H. Ye, C.-S. Tang, and P.-Y. Wang, "Resonant analysis of magnetic coupling wireless power transfer systems," *IEEE Trans. Power Electron.*, vol. 34, no. 6, pp. 5513–5523, Jun. 2019, doi: 10.1109/TPEL.2018.2868727.
[32] J. Jiang, X. Dai, and A. P. Hu, "A dynamic tuning method for ZPA frequency operation of MEU-WPT system by DC input voltages regulation," *IEEE Trans. Power Electron.*, vol. 37, no. 9, pp. 11369–11381, Sep. 2022.
[33] F. W. Grover, *Inductance Calculation: Working Formulas and Tables*. New York, NY, USA: Dover, 1946.
[34] S. Raju, R. Wu, M. Chan, and C. P. Yue, "Modeling of mutual coupling between planar inductors in wireless power applications," *IEEE Trans. Power Electron.*, vol. 29, no. 1, pp. 481–490, Jan. 2013.

Xiaomin Wang received the B.E. degree in automation from the Qingdao University, Shandong, China, in 2019. She is currently working toward the Ph.D. degree in control theory and control engineering with the College of Automation, Chongqing University, Chongqing, China.

Her current research interests focus on wireless power transfer network (WPTN) and the application of artificial intelligence (AI) in wireless power transfer technologies.

Xin Dai (Member, IEEE) received the B.S. degree in industrial automation from Yuzhou University, Chongqing, China, in 2000, and the Ph.D. degree in control theory and control engineering from the School of Automation, Chongqing University, Chongqing, China, in 2006.

In 2012, he was a Visiting Scholar with The University of Auckland, Auckland, New Zealand. He is currently working as a Professor with the School of Automation, Chongqing University. His research interests include inductive power transfer technology and nonlinear dynamic behavior analysis of power electronics.

Shunsheng Hong received the B.E. degrees in aircraft power engineering from the Civil Aviation Flight University of China, Guanhan, China, in 2019, and the M.Sc. degree in control science and engineering from the Chongqing University, Chongqing, China, in 2023. He is currently working toward the Ph.D. degree in control theory and control engineering with Chongqing University, Chongqing, China.

His current research interests include the wireless power transfer and power electronics.

Yanling Li received the B.Sc. degree in automation from YuZhou University, Chongqing, China, in 2000, and the M.Sc. degree in signal and information processing from University of Electronic Science and Technology, Chengdu, China, in 2007, and the Ph.D. degree in control science and engineering from Chongqing University, Chongqing, China, in 2017.

She is currently an Associate Professor with School of Electrical Engineering and Electronics Information, Xihua University. Her research interests include wireless power transfer technology and control theory and application.

Udaya Kumara Madawala (Fellow, IEEE) received the B.Sc. degree (*Hons*.) in electrical engineering from the University of Moratuwa, Moratuwa, Sri Lanka, and the Ph.D. degree in power electronics from the University of Auckland, Auckland, New Zealand, as a Commonwealth Doctoral Scholar.

He is currently a Full Professor. His research interests include power electronics, wireless power transfer, renewable energy, permanent magnet motor drives, and vehicle-to-grid applications.

Prof. Madawala is a Distinguished Lecturer of the IEEE Industrial Electronic Society. He has served both the IEEE Power Electronics and Industrial Electronics Societies in numerous roles, relating to editorial, advisory, conferences, administrative and technical committees, and chapter activities.